POLITECNICO
MILANO 1863

SCUOLA DI INGEGNERIA INDUSTRIALE
E DELL'INFORMAZIONE

Executive Summary of the Thesis

High-Speed Label-Free 3D Biomedical Imaging through Multiphoton and Broadband CARS Microscopy

Laurea Magistrale in Physics Engineering - Ingegneria Fisica

Author: Matteo Mandelli

Advisor: Prof. Dario Polli

Co-advisor: Dr. Federico Vernuccio

Academic year: 2022-2023

1. Introduction

The most common and affirmed tools for biomedical imaging to produce detailed chemical maps are fluorescence microscopy and vibrational microscopy. Fluorescence microscopy is well-known and widely adopted due to its incredible sensitivity and the variety of fluorescent markers. These markers can be endogenous when naturally present in the sample or exogenous when added externally. However, endogenous markers are finite and are not enough to fully study cells and tissues, and exogenous markers may lead to sample perturbation. Another limitation to deal with is the number of times a given area of the sample can be imaged due to photobleaching or the limited amount of marker "colours" we can distinguish before their broad emission spectra overlap. These limitations call for a technique that can image biological samples in a label-free and non-destructive way.

Vibrational microscopy overcomes these limitations since it enables to distinguish different biological compounds in heterogeneous samples by the detection of their characteristic vibrational spectrum, making it a non-invasive and label-free technique.

One approach to vibrational microscopy is vibrational absorption microscopy. However, this technique has limited spatial resolution and penetration depth since it uses mid-infrared light (MIR). These issues make this technique unsuitable for imaging intricate biological samples.

Raman microscopy instead uses near-infrared (NIR) light, which overcomes these limitations, making it an ideal technique for biological applications. Spontaneous Raman (SR) is the most common method in this field and it utilizes a quasi-monochromatic visible or Near Infrared (NIR) pump laser beam with frequency ω_p. The vibrational information is encoded in the spontaneously emitted and inelastically scattered Stokes or anti-Stokes components, with frequencies $\omega_S = \omega_P - \Omega$ and $\omega_{aS} = \omega_P + \Omega$, respectively. With Ω representing the vibrational resonance of the sample.

Due to its chemical specificity, there are already plenty of applications where SR is used in the biomedical field. However, SR still is not the ideal technique for high-speed imaging since it suffers from a low scattering cross-section thus requiring long integration times (ranging from approximately 100 ms to 1 s) for the acquisition of a single-pixel vibrational spectrum.

Coherent Raman Scattering (CRS) techniques can overcome the limitations of SR by using light pulses to create and detect a vibrational coherence within the molecules in the laser focus. A collective molecular oscillation is induced by using two spatially and temporally synchronized pulses, the pump at frequency ω_p and the Stokes at frequency ω_S. This results in all molecules vibrating in phase when the difference between pump and Stokes frequencies matches a characteristic vibrational frequency Ω_R, that is, $\omega_P - \omega_S = \Omega_R$. This vibrational coherence significantly enhances the Raman response compared to the incoherent SR process. Furthermore, as a non-linear microscopy technique, CRS generates signals only in the focal volume, exhibiting 3D sectioning capabilities without the need for confocal apertures.

The two most commonly employed CRS implementations are stimulated Raman scattering (SRS) and coherent anti-Stokes Raman scattering (CARS). Stimulated Raman Scattering (SRS) measures either the intensity gain of the Stokes beam or the intensity loss of the pump beam. On the other hand, Coherent Anti-Stokes Raman Scattering (CARS) detects the signal at the anti-Stokes frequency $\omega_{aS} = \omega_P + \Omega$ with intensities up to 7 orders of magnitude greater than SR signals [2].

However, this implementation of CARS (called single-frequency or narrowband CARS) has a major limitation, it is fast compared to SR but it also only probes one vibrational mode at a time so it has limited information content. Broadband CARS instead address this issue by combining narrowband pump pulses with broadband Stokes pulses to generate a broadband anti-Stokes component, enabling the recording of broad vibrational spectra at once.

This thesis will focus both on thoroughly testing the capabilities of broadband CARS as well as improving the experimental setup by transforming it into a multimodal microscope. In particular, the new channel will be used for second harmonic generation (SHG) and three-photon excited fluorescence (3PEF) as they are also label-free techniques that can provide different information with respect to CARS. Therefore we will analyze in detail the experimental setup, the data processing pipeline and several experiments.

2. Experimental Setup

The experimental setup used [3, 4] can be seen in figure 1. For its description I will divide it into three key parts according to their purpose: Light generation, microscope and signal detection.

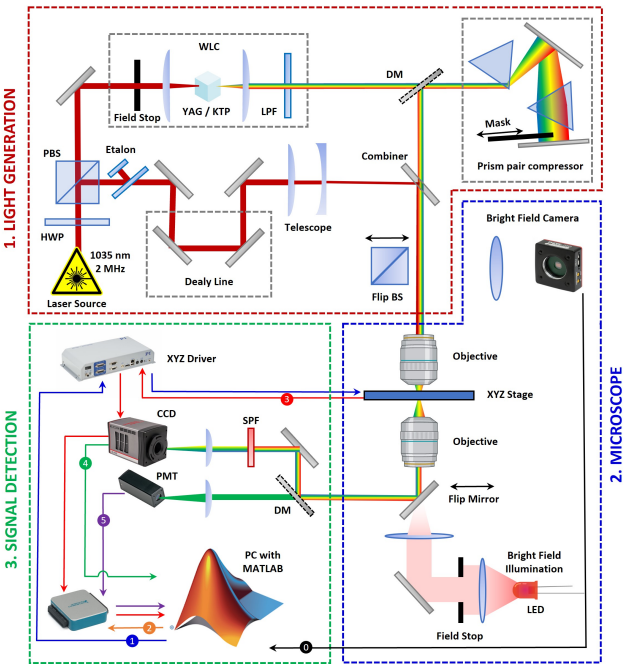

Figure 1: Simplified representation of the experimental setup. Note that the propagation of the laser beam starts in red and remains red for the Pump while the Stokes is represented with multiple colours as the pulse gets broadband. I also reported the components that would be flipped for Brightfield (BF) even if the BF light here is interrupted by the flip mirror. Additionally, at the bottom of the image, we can see the cables connecting each peripheral to the computer running Matlab where each step where data is transferred from or to a component is represented with a different colour.

2.1. Light Generation

Starting from the light source our system uses a fibre-based ytterbium laser (Monaco 1035, Coherent) that delivers pulses of 270 fs duration and 10nm bandwidth centred around $\lambda_0 = 1035$ nm. The laser beam is then split into two using a half-waveplate (HWP) and polarizing beam splitter (PBS) system. The first replica will generate pump pulses while the second broadband Stokes pulses. The first replica with an average power of roughly 2 W passes through a high-finesse Fabry-Perot etalon that narrows

the spectral bandwidth to a FWHM of 0.9 nm which corresponds to 9 cm^{-1} for $\lambda = 1035$ nm. Then it encounters a delay line to adjust the temporal overlap with the second replica after which it is combined with it and focused onto the sample by an objective. The second replica instead is focused onto a 10mm crystal (either YAG or KTP) to generate a White-Lite Continuum (WLC). After the WLC a long-pass filter (LP1050, Thorlabs) is employed to select only the red-shifted light and a prism pair compressor compensates for the chirp. The generated Stokes pulses are then combined and focused onto the sample together with the pump pulses. Once at the sample plane, they will exhibit a sub-20 fs pulse duration with a bandwidth ranging from 1200 nm to 1600 nm. Note that the fine-tuning of this bandwidth is done by inserting a mask in the prism compressor where the different colours travel in parallel.

2.2. Microscope

The microscopy unit adopts a confocal microscope in an upright configuration that uses a pair of 100x air objectives with high Numerical Aperture (NA) (Olympus LCPLN100XIR, NA=0.85). Sample scanning is accomplished using two translational stages stacked one on top of the other, one for fine adjustments along X,Y and Z directions and the other to perform raster scanning. Additionally, the microscope is equipped with a bright-field microscopy system to visualize the field of view that needs to be imaged using BCARS. A LED serves as the light source, and a lens configuration, consisting of two objectives and another lens, creates a pseudo-Kohler illumination system. Finally, a camera (Thorcam, Thorlabs), positioned in the image plane, allows us to capture wide-field images of the sample.

2.3. Signal Detection

Finally, part of the signal will pass through a long-pass dichroic mirror (FF757-DI01) and a short-pass filter (SP1000, Thorlabs) that blocks the pump before entering a spectrometer and CCD camera combination. The rest of the signal reflected by the dichroic mirror will also be filtered before entering the Photomultiplier Tube Module. The filter changes whether we acquire SHG or 3PEF.

At this point, we need to follow the electrical signals shown in 1 in the signal detection part. The very first signal acquired is from the Bright-field before the actual measure. Then Matlab controls the stage through its driver (signal 1) to initiate the scanning and at the same time start acquisition with the DAQ (signal 2). Once the stage moves it sends a signal back to its driver (signal 3) which sends a trigger to the CCD to acquire a spectrum. The CCD itself then sends a trigger to the DAQ once it starts acquiring. At the same time, the CCD also sends the acquired spectra to Matlab through a USB interface. During the whole measure, the DAQ records the triggers from the camera and the PMT signal (signal 5) which is acquired continuously. This way when the scanning ends Matlab can read the triggers and the PMT signal registered by the DAQ to select just the intervals coinciding with each pixel acquisition of the CCD.
This approach allows the acquisition of images at very high speeds, utilizing the minimum exposure time allowed by the CCD camera which is 0.8 ms. Moreover, each pixel can be associated with a specific spatial position, without encountering any motion artifacts or shifts in the rows of the acquired images.

3. Acquisition and Data Analysis

The procedure to obtain the chemical maps mentioned in section 1 requires first the acquisition of all the necessary signals and afterwards the data processing.
The **acquisition** procedure comprises three main steps:

- Preliminary measurements: They include the acquisition of dark, non-resonant background (NRB) and toluene spectra. The dark will be used to remove the RMS noise due to the dark counts of the CCD, the NRB for NRB removal afterwards, and the tolouene spectra to calibrate the wavenumber axis using another reference toluene spectra.
- Bright-field image: It is useful to find specific features in large samples and also to focus the laser beam exactly on the part of sample where we want to fine-tune the CARS signal later.

- Multichannel acquisition: It is the actual measurement that can take place after the others are completed. It includes the B-CARS signal acquired from the CCD and the PMT channel that in our case is used either for SHG or 3PEF.

Once we have acquired the necessary data we can continue with the **data processing** as follows:

- White noise reduction: The signal will present white noise due to the inherent dark noise of the CCD, to remove it I use Singular Value Decomposition on an Anscombe-transformed spectra [1].
- Non-Resonant Background removal: The signal will also be distorted by NRB, so we will remove it using a time-domain Kramers-Kronig algorithm [1].
- Directional denoising: The signal presents artefacts in the shape of vertical or horizontal lines induced by fluctuations of the laser source. I removed these lines using directional denoising with Fourier Spectrum Cloning.
- Spectral unmixing: After the signal has been denoised we can apply different spectral unmixing algorithms to distinguish the different chemical components. In our case, we focus on the N-FINDR and K-Means algorithms implemented in the RamApp software (https://beta.ramapp.io).

4. Experiments and Results

The experiments carried out during this thesis focused on assessing the capabilities and limits of the multimodal microscope presented in section 2. We started with simple test samples of plastic beads immersed in a solvent, then we moved on to more complex biological samples and measures. We concluded with time-delayed CARS measurements on crystalline samples to measure the population lifetime of the main vibrational modes, showing the versatility of the B-CARS system.

4.1. Test Samples

The chosen sample was a mixture of 8 μm polymethylmethacrylate (PMMA) and 10 μm polystyrene (PS) beads immersed in dimethyl sulfoxide (DMSO) and sandwiched between two 170 μm quartz coverslips. The results after white noise reduction, NRB removal, directional denoising and spectral unmixing can be seen in figure 2.

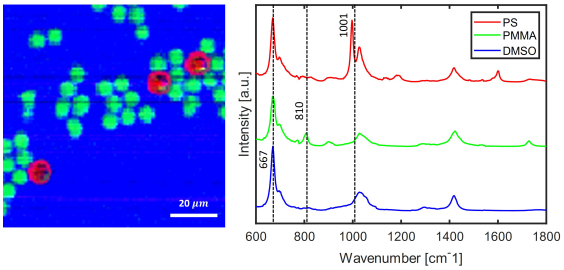

Figure 2: False colour image and spectra of the endmembers found with N-FINDR algorithm.

We can distinguish the three components of the sample both in the false colour image and in the spectrum where the relevant peaks for each species are highlighted.

4.2. 3D Sectioning on Spheroids

The following experiment aimed to test the 3D sectioning capabilities of B-CARS on spheroids, 3D dimensional aggregates that mimic the characteristics of cell aggregates such as microtumors. The false colour images obtained after the denoising procedure at different focal planes can be seen in figure 3 where we were able to identify cytoplasm and nuclei.

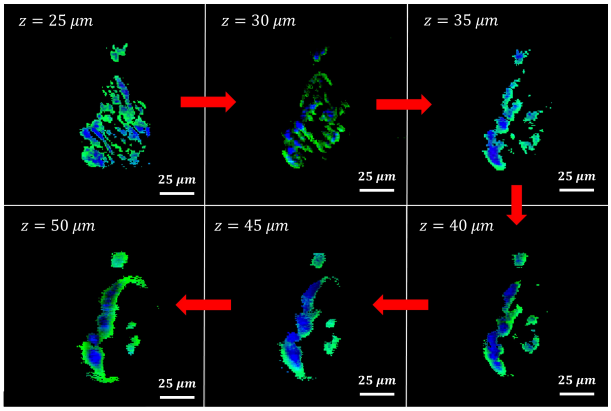

Figure 3: False colour image obtained with N-FINDR at different focal planes. The green endmember represents cytoplasm and the blue one nuclei.

We identified the two endmembers as nuclei and cytoplasm from their spectra, reported in figure 4, where we can see in the CH region two peaks characteristic of proteins and lipids. In-

deed nuclei are richer in proteins while cytoplasm is richer in lipids.

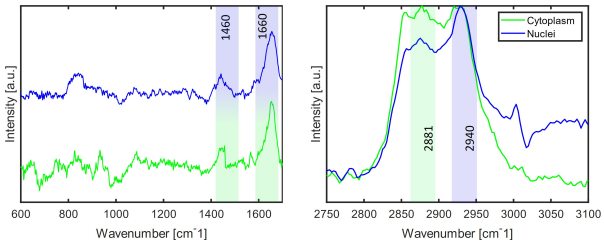

Figure 4: False colour image obtained with N-FINDR at different focal planes.

The other peaks highlighted in the fingerprint region are the amide I and amide III peaks which are present in both endmembers. So to confirm our hypothesis we also plotted at each focal plane only the ratio between the two peaks in the CH region, obtaining an almost identical result (see figure 5) to the one found with the unmixing procedure.

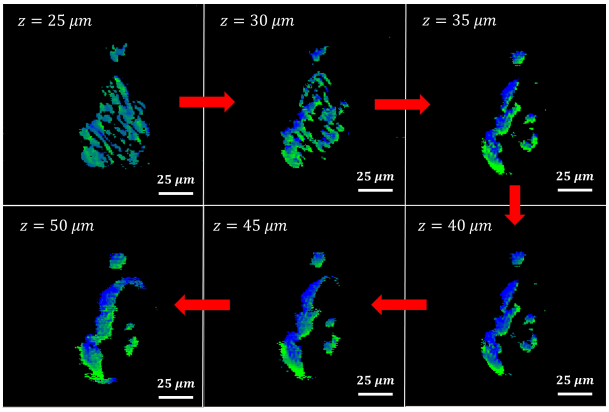

Figure 5: Dual colour CARS image of the ratio between peaks A ($2881 cm^{-1}$) and B $2940 cm^{-1}$.

4.3. Multichannel detection on Microcalcifications

The next study concerned tumoral breast tissue containing mammary microcalcifications (MCs), and it was analyzed with CARS in conjunction with SHG and 3PEF. Initially, we concentrated on testing the SHG acquisition. In this phase, we used B-CARS to identify proteins and lipids while SHG identified collagen, see figure 6. Note that collagen being a protein is mostly located in the same position as the red protein-rich endmember which is expected.

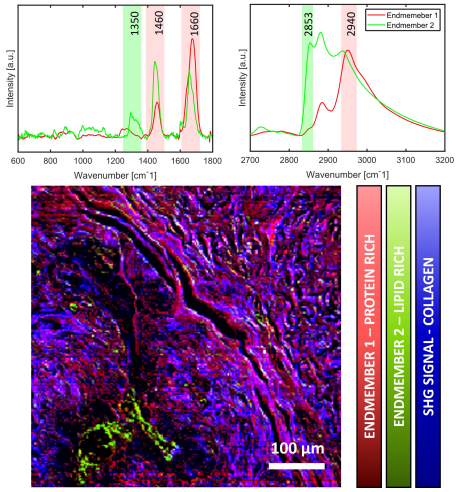

Figure 6: False colour image reconstructed from SHG and endmembers signals.

Then we focused on MCs and in particular on distinguishing them from the tissue. We noticed that since MCs transmit less light they are sometimes identified due to the peak of hydroxyapatite around 960 cm^{-1} and sometimes due to their weaker signal. However, in conjunction with SHG and 3PEF, we were able to double-check our results as we can see from figure 7. First MCs are identified in Bightfield as darker areas. Then B-CARS identifies tissue (usually with lipid-rich and protein-rich endmembers in red and blue) and MCs (with the hydroxyapatite peak or weaker signal in green). SHG instead identifies collagen and ignores MCs so we used it to check the B-CARS data. Finally, 3PEF identifies the metabolic cofactors NADH and FAD which are present in all tissues, so it can also be used as a control for B-CARS.

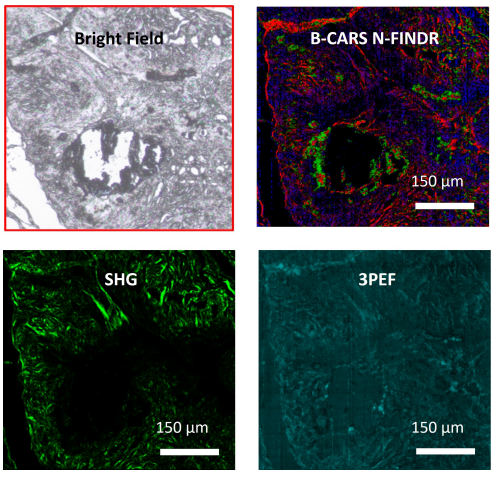

Figure 7: Set of images taken with different techniques in the same position.

4.4. Time-Delayed CARS on Crystals

In this final experiment, I used time-delayed CARS to calculate the build-up and decay times of NRB in glass (see figure 8) as well as the decay times of resonant signals in diamond and potassium titanyl phosphate (KTP). Both build-ups and decays were calculated fitting an intensity curve for one or multiple Raman shifts as shown in figure 9.

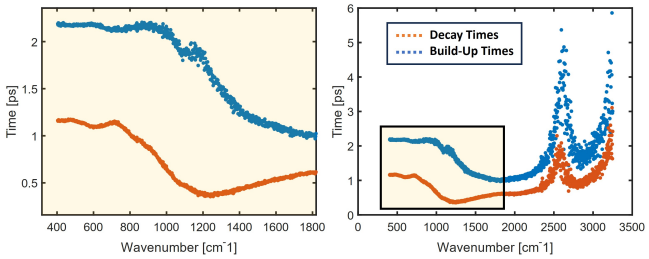

Figure 8: Build up and decay times in glass.

Diamond has only one peak centred at 1336 cm^{-1} so we fitted the signal only at that Raman shift (see figure 9). The build-up and decay times found for NRB were in line with the ones found for glass (1.06 and 0.48ps), while the decay of the resonant peak was 6.33ps, close to the expected phonon lifetimes reported in the literature which range from 5.6ps to 6.0ps.

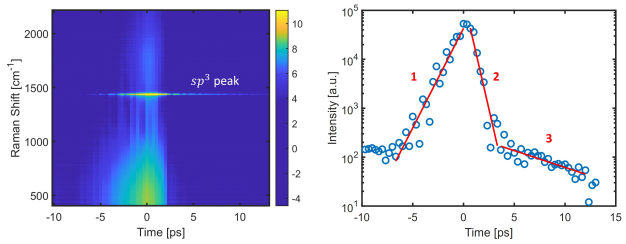

Figure 9: Left: TD-CARS of diamond. Right) fitted exponential at 1336cm^{-1} showing build-up (1) and double decay and of NRB (2) and resonant peak (3).

KTP instead presented several peaks. NRB build-up and decay times of each one were in line with the first result obtained with glass, while decay times of the resonant peak resulted to be within an order of magnitude with what was reported in the literature.

5. Conclusions

In this thesis, I was able to show how our B-CARS setup has proven to be a powerful tool for biomedical imaging and cancer research since it provides a label-free and non-invasive way to probe the molecular details of living tissues. The evolution of the system in a multimodal microscope allowed also to complement B-CARS imaging with other techniques such as SHG and 3PEF that further extended the functionality of the system.
Future developments for our setup may focus not only on improving its capabilities but also on adding user-friendly features to simplify the operation of the setup and increase reliability for potential commercialization. This would make B-CARS accessible and applicable in clinical settings, where it could be used to identify and characterize tumours and other complex biological structures.

References

[1] C. H. Camp Jr, Y. J. Lee, and M. T. Cicerone. Quantitative, comparable coherent anti-stokes raman scattering (cars) spectroscopy: correcting errors in phase retrieval. *Journal of Raman Spectroscopy*, 47(4):408–415, 2016.

[2] D. Polli, V. Kumar, C. M. Valensise, M. Marangoni, and G. Cerullo. Broadband coherent raman scattering microscopy. *Laser & Photonics Reviews*, 12(9):1800020, 2018.

[3] F. Vernuccio, A. Bresci, B. Talone, A. de la Cadena, C. Ceconello, S. Mantero, C. Sobacchi, R. Vanna, G. Cerullo, and D. Polli. Fingerprint multiplex cars at high speed based on supercontinuum generation in bulk media and deep learning spectral denoising. *Optics Express*, 30(17):30135–30148, 2022.

[4] F. Vernuccio, R. Vanna, C. Ceconello, A. Bresci, F. Manetti, S. Sorrentino, S. Ghislanzoni, F. Lambertucci, O. Motiño, I. Martins, et al. Full-spectrum cars microscopy of cells and tissues with ultrashort white-light continuum pulses. *The Journal of Physical Chemistry B*, 2023.